44th AIAA Aerospace Sciences Meeting and Exhibit
9 - 12 January 2006, Reno, Nevada

AIAA 2006-962

Measurements and Modeling of the Flow Field in an Ultra-Low Emissions Combustor

Gopalakrishnan, P.[*], Undapalli, S.[*], Bobba, M.[*], Sankaran, V.[§], Menon, S.[†], Zinn, B. T.[**], Seitzman, J.[‡]

School of Aerospace Engineering

Georgia Institute of Technology

Atlanta, GA 30332

The flowfield of a novel combustor design that can operate stably even at high flowrates and very lean conditions is studied. This Stagnation Point Reverse Flow (SPRF) combustor consists of a central injector at the single open end of a cylindrical chamber, with the injector inlet area much less than the open area of the combustor through which the exhaust products leave. Thus the flowfield can be characterized as a confined jet in an opposed flow. Experiments with Particle Image Velocimetry (PIV) as well as computations employing Large Eddy Simulations (LES) have been used to characterize the nonreacting and reacting flowfields within the combustor for premixed and nonpremixed modes of operation. Both nonreacting and reacting cases exhibit a "stagnation" region with local average and high fluctuating velocities. The reacting flows exhibit higher mean and fluctuating velocities than the nonreacting flow. The nonreacting flow stagnates earlier than the reacting flow due to the effects of gas expansion in the reacting flow case. Consequently, the jet decay rates are higher for the reacting flows. The high shear between the forward and reverse flows causes significant recirculation, resulting in enhanced entrainment and mixing of the returning hot product gases into the incoming reactant jet. Comparison of the instantaneous flowfields reveals that the reacting jets exhibit significant lateral motion and distortion compared to the nonreacting case. This parallels the large increase in fluctuating velocities and turbulence intensities that coincide witht the region of high heat release. Nonpremixed and premixed reacting flowfields at the same fuel and air mass flow rates are found to be very similar except in the near field region of the jet, due partly to the lack of heat release there in the nonpremixed case.

I. Introduction

Environmental concerns and legislative regulations are driving combustor manufacturers to meet increasingly more stringent emission standards while maintaining (or improving) efficiency and reliability. For example, reductions in NOx emissions from land-based, gas turbine combustors have been achieved mainly through lean premixed/partially premixed combustion, dilution with exhaust gases and staged combustion, all of which lower peak flame temperatures and consequently NOx emissions. In the most common approach, premixed (or partially premixed) combustion however, combustor static and dynamic stability is compromised as the mixture is made leaner. This results from the weaker combustion process, which is more vulnerable to small perturbations in combustor operating conditions.[1]

[*] Graduate Research Assistant (AIAA student member)
[§] Post Doctoral Fellow (AIAA member)
[†] Professor (AIAA Associate Fellow)
[**] Davis S. Lewis Jr. Chair and Regents' Professor (AIAA Fellow)
[‡] Associate Professor (AIAA Associate Fellow)

A new design, known as the stagnation point reverse flow (SPRF) combustor,[2] has recently been developed to address these issues. The unique design of this combustor allows it to burn gaseous or liquid fuels in premixed or nonpremixed modes of combustion with low NOx and CO emissions. The combustor consists of a tube with one end open and the other closed. Contrary to most combustors, the reactants and products enter and leave this combustor at the same (open) end. In the investigated configuration, the reactants are injected along the combustor center line, moving towards the closed end. Products leaving the combustor can internally preheat the reactants coming in through the injector thereby enhancing stability and facilitating leaner operation of the combustor. For premixed operation, a single reactant jet enters the combustor. For nonpremixed combustion, fuel enters through a central jet surrounded by an annular air jet.

While there is a significant amount of literature on free turbulent jets, confined jets, jets with coflow, jets exiting onto impingement plates and jets in cross-flow, there appears to be little or no previous flowfield studies on a geometry resembling this combustor, with its self-reversing flow. Since the SPRF design does incorporate features of may of the jet flows mentioned above, some background about these flows is presented here.

Early experimental work on turbulent free jets over the whole range of Froude numbers from momentum dominated jets to the pure plume have been reviewed in depth and similarity and scaling laws have been developed.[3,4] The following quantities have been identified as important parameters in quantifying jet flows: rate of spread, later and longitudinal profiles of average velocity, temperature and species concentration, turbulent quantities such as fluctuating velocity, turbulent shear and entrainment/mixing characteristics.[3-6]

The effect of confinement and co-flowing streams (external mean velocity) on the structure of axisymmetric turbulent jets has also been studied. Borean *et al*.[8] observed that the variation of the mean velocity and the rate of expansion of the jet are identical to that of a free jet, which suggests that the inner flow (jet) is not affected by the external flow. A similar result was obtained for the turbulent quantities where only some of the third order moments exhibit a different behavior near the axis of the flow. In the case when there is no external coflow velocity, the effect of confinement changes the structure of the jet significantly. In a study of laminar confined rectangular jets (without coflow)[9], it was found that the decay rate of the confined jet is almost three times less than that of square and circular free jets but is greater than that of plane free jets by 10–30%. The spreading rate of the confined jet was observed to be quite similar to that of the plane free jets but higher than the circular and square free jets. The authors concluded that the decay rate of the confined jet follows a two-dimensional type of flow more closely rather than a three-dimensional flow.

It is also known that density has a considerable effect on the near field turbulence values of jets.[10,11] Variable density jets such as those encountered in free turbulent jet flames have different entrainment characteristics - lighter gases are entrained more easily. Some studies have been also conducted on confined jet flows impinging on stagnation plates. The amount of air entrained by the jet is linked to the density ratio, the length of jet development and also to the pressure gradient due to the impact on the plate.[12] It was also found that the entrainment rate is highest when the stagnation plate is located approximately 10 jet diameters from the nozzle exit.This configuration is often found in burner geometries that produce flat stagnation flames. The SPRF combustor however differs from this geometry because of the increased distance of the jet exit from the stagnation plate (25 annular diameters in the implementation studied here), and because the impingement plate is located within the confining walls of the system. It should also be noted that definition of entrainment for free and confined, non-coflowing jets is usually based on the increase in mass flowrate caused by the drag of the jet. This definition, however, lacks a clear meaning in the context of confined coflowing jets where mass flowrate is fixed.

The SPRF combustor when operated in nonpremixed mode adds an additional feature to the flow – the fuel and air form a pair of coaxial confined jets. Extensive literature exists on flow features of free coaxial jets. The most important parameter influencing jets with coaxial flow has been identified as the momentum ratio between the inner and annular flows.[13-15] Villermaux and Rehab[16] suggest that in coaxial jets with outer to inner velocity ratio higher than unity, the two parameters controlling the mixing process are the initial vorticity thickness of the outer, fast stream, and the elongation rate based on the velocity difference between the two streams and the gap thickness of the annular jet. However, little is known about the effects of confinement on coaxial jets. Another unusual aspect of the SPRF flowfield is that the entering reactant jet is faced with an opposed flow produced by the reversal of the jet fluid at the stagnation region in front of the closed end. Previous research in this area has been limited to single jets in opposed flows where the two flows are uncoupled, e.g., a jet injected upstream into a wind tunnel. Studies show that there exists a characteristic jet penetration length before the jet turns around which can be derived based on empirical relations.[17,18] It was found that the turbulent mixing process in this configuration depends on the velocity profiles at the nozzle exit and the excess momentum of the jets.

As noted previously, the SPRF combustor design represents a unique blending of these various jet flows, and there are no previous experimental, computational or analytic studies of such a flow. Therefore to characterize the

SPRF flowfield and provide a basis for understanding its operation, this paper describes a combined experimental and computational study that employs PIV (particle image velocimetry)[19] and LES (large eddy simulations).[20]

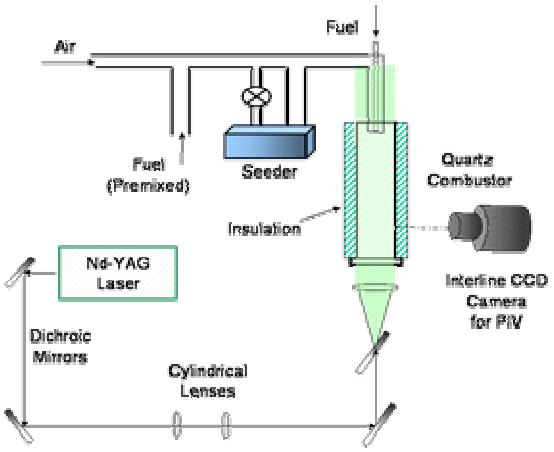

Figure 1. Schematic of experimental set-up.

II. Experimental Set-Up

The SPRF combustor used for the current work is a laboratory scale, atmospheric pressure device. It consists of a dual concentric tube injector (12.5 mm outer diameter) centrally located in a 70 mm inner diameter quartz tube, which is closed at the bottom end with a quartz disk (Figure 1). The base plate is fit snugly inside the quartz tube so that there is no measurable leakage of fuel/air through the closed end. The design of the injector allows for easy switching between premixed and nonpremixed modes of operation. The inner tube is centered with respect to the outer injector annulus with the help of three set-screws. A premixed natural gas-air mixture is injected through the injector's annulus in premixed operation. In the nonpremixed mode, fuel is injected through the inner tube and air through the annulus; no fuel-air mixing can occur until the flows enter the combustor. Care is also taken to ensure that the co-annular injector is centered with respect to the combustor. In the premixed mode of operation, the fuel is injected well upstream of the injector exit to ensure proper premixing of the fuel and air. Fuel and air flow rates are controlled separately with calibrated rotameters. The combustor is insulated with a close fitting, hollow alumina cylinder cut into four sections. To facilitate optical access, a 150° window is cut out of one of the sections, which can be placed at different axial locations. Thus the optical measurements are acquired one-quarter of the combustor at a time, and the complete field is derived by assembling them. The temperature of the reactants and the exhaust gases can be monitored with an unshielded K-type thermocouple. The thermocouple is not present while the imaging measurements are being recorded.

Measurements of the two-dimensional velocity field are obtained with a typical PIV system consisting of a seed particle generator, a source of illumination, and an imaging system. The seed particles are generated using a fluidized bed particle generator with an air turbine vibrator, and 1-2 micron aluminum oxide flakes are used as seed material. The particles are baked beforehand to prevent agglomeration. The tracer particles are illuminated with a light sheet produced with the second harmonic (532 nm) output of a dual head pulsed ND:YAG laser. Each laser head is capable of providing pulse energies of 150 mJ at a rate of 10 Hz. The beams from the two heads were aligned so as to ensure that there is better than 90% overlap between the two laser sheets. Since the laser pulse is very short (FWHM of 8ns) it can effectively freeze flow motion even at supersonic velocities. The beam is then converted into a thin sheet (~0.4 mm thick) 65 mm wide with two cylindrical lenses. The laser sheet enters the combustor through the quartz base plate. The correlated pairs of particle scattering images are acquired with a 12-bit interline CCD camera (MicroMAX, 1300x1030 pixels) equipped with a 50 mm Nikkor lens (f 1/1.8). The timing between the two laser heads is synchronized with the camera shutter with an external pulse generator (SRS – DG535). For the current measurements, the pulse energies for the two lasers were nearly 90 mJ, and the pulse delay between the image pairs was varied from 3-11 microseconds. The data is collected in 55 x 89 mm regions of the combustor and then assembled together to produce complete flow field. A commercial software package (Insight 6, TSI) is used to calculate the velocity field. First, the raw PIV images are preprocessed to remove background noise, for example from wall scattering. In order to prevent an unacceptably large background scattering signal caused by deposition of the seed material on the combustor walls, the combustor was cooled and cleaned after every 50 image pairs. An FFT based cross-correlation technique is employed to find the average particle displacement in a 64 x 64 pixel region with a 50% overlap in the interrogation areas yielding a total of 1209 velocity vectors. The data was also processed with varying sizes of interrogation areas to eliminate any biasing of the velocity vectors. The particle displacements are obtained with a 0.1 pixel accuracy using a Gaussian sub-pixel interpolation algorithm. Each vector represents the average velocity in an interrogation volume 2.19 x 2.19 x 0.4 mm.

III. Numerical Method and Boundary Conditions

Favre filtered, unsteady, compressible, Navier-Stokes equations for conservation of mass, momentum, energy and species are solved along with an equation for subgrid kinetic energy in the present study. The equation for the transport of subgrid kinetic energy is based on the non-equilibrium transport model of Schumann *et al*.[21] The system of conservation equations are supplemented by equations of state and other constitutive relations for the transport properties. A LES methodology[21,22] is used to solve the filtered, unsteady, compressible Navier-Stokes equations in generalized coordinates. The numerical algorithm uses a finite-volume scheme that is second-order accurate in space and time. The computational domain is resolved using 112 x 75 x 57 grid points along, the axial, radial, and azimuthal directions, respectively. Grid clustering was employed in regions of high gradients (such as the jet shear layer and near the walls). Inflow and outflow boundary conditions were set using the characteristic conditions of Poinsot and Lele.[23] On all solid walls, no-slip conditions were prescribed for the velocity field. Non-catalytic wall boundary conditions were used for the species field. The temperature at the walls was set as adiabatic or cold boundary conditions for the reacting and nonreacting flows respectively. In the present studies, the turbulence-chemistry interaction at the subgrid level is modeling with eddy-break-up approach.[24] This model includes the sub-grid mixing effects on the assumption that the combustion process are either kinetically controlled or mixing controlled (depending the relative time-scales between them). As a result, at any instant the reaction rate is computed as the minimum of the kinetic reaction rate and the mixing rate. This is explained as follows:

For a general reaction mechanism comprising of N_r reactions given by

$$\sum_{k=1}^{N_s} \nu'_{k,j} M_{k,j} \longleftrightarrow \sum_{k=1}^{N_s} \nu''_{k,j} M_{k,j}$$

the filtered reaction rates for species ``k'' is computed as

$$\overline{\dot{w}} = W_k \sum_{j=1}^{N_r} (\nu''_{k,j} - \nu'_{k,j}) \min[q_j^{mix}, q_j^{kin}]$$

where q_j^{mix} and q_j^{kin} are the molar reaction rates based on mixing and Arrhenius chemical kinetic rate, respectively. The Arrhenius reaction rates for step ``j'' is given by,

$$q_j^{kin} = k_{f,j} \prod_{k=1}^{N_s} [M_k]_{k,j}^{\nu''} - k_{b,j} \prod_{k=1}^{N_s} [M_k]_{k,j}^{\nu'}$$

and the mixing rates for the forward and the backward reactions are given by

$$q_{j,f}^{mix} = \frac{1}{\tau_M} \min\left(\frac{[M_k]}{\nu''_{k,j}}\right) \text{ and } q_{j,b}^{mix} = \frac{1}{\tau_M} \min\left(\frac{[M_k]}{\nu'_{k,j}}\right)$$

Here, τ_M is the mixing time scale and is related to the sub-grid turbulence by $\tau_M = C_{EDC} \dfrac{\overline{\Delta}}{\sqrt{k^{aga}}}$.

The most severe draw-back of the eddy-break up approach is the use of heuristic non-universal calibration constants. This approach has been considered in the simulations because of its simple implementation and it was also shown to correctly reproduce global features in flows similar to that of SPRF combustor.[25] Thus the authors are aware of the limitations of the EBU combustion model employed, but the intent here is to examine the general flow features and turbulence-heat release interactions, but is not meant to predict exact flowfield parameters.

The combustion-chemistry model uses a two step, six species reduced mechanism.[26] The two reaction steps are:

$$CH_4 + O_2 \rightarrow CO + H_2O$$
$$CO + \tfrac{1}{2} O_2 \rightarrow CO_2$$

The first step includes the partial oxidation of fuel, and the second step models the final oxidation of CO. The boundary conditions in the simulations are set so that they match the experimental conditions as accurately as possible. For the non-reacting case, a jet of air at atmospheric pressure and temperature flows into the combustor at a volumetric flow rate of 0.00714 m^3/s. This value is matched in the simulations with a fully developed turbulent inlet velocity profile with an average velocity of 73 m/s. An RMS velocity profile with 5% intensity has been superimposed on this mean velocity profile. Identical mass flow rates are also used in the case of reacting case but with a premixed jet of methane and air with an equivalence ratio of 0.58. Temperature data collected in the experimental set-up shows that the injected mixture is preheated to ~500 K by exiting product gases before the mixture leaves the injector. Hence in the simulations, the premixed jet was fixed with an average velocity of 129 m/s and a temperature of 500 K in order to maintain the same mass flow rate.

IV. Results and Discussion

Nonreacting and Premixed Reacting Flow

The time-averaged flowfield, based on 300 instantaneous PIV images, is shown in Figure 2 as a combination of axial velocity contours and interpolated streamlines for both nonreacting and premixed reacting flows. It should be noted that the streamlines may appear discontinuous in some locations. This is because the streamlines are interpolated for each quarter of the combustor (since the data is acquired separately) and then assembled together. The results were obtained for a total mass flow rate of 8.1 g/s in both the non-reacting as well as the reacting flow cases. For the nonreacting flow, the incoming gas is composed only of air; while for the reacting case, it is composed of premixed natural gas and air with an equivalence ratio of 0.58. Figure 2a shows the average axial velocity contours for the nonreacting flow. The flow at the exit of the injector is an annular jet entering into the combustor. In experiments, the central tube was closed (for nonreacting and premixed reacting flow cases) upstream to prevent any flow through it. This creates a cylindrical cavity into and out of which the combustor gases can flow and circulate. To simulate this in the computations, the cylindrical cavity is included in the grid model. But to reduce the computational cost, the length of the cavity is restricted to be equal to 12.5mm (one annular diameter). In some ways, the overall flowfield resembles that of a confined jet, but the presence of the end plate causes the axial velocity to decay quite rapidly.

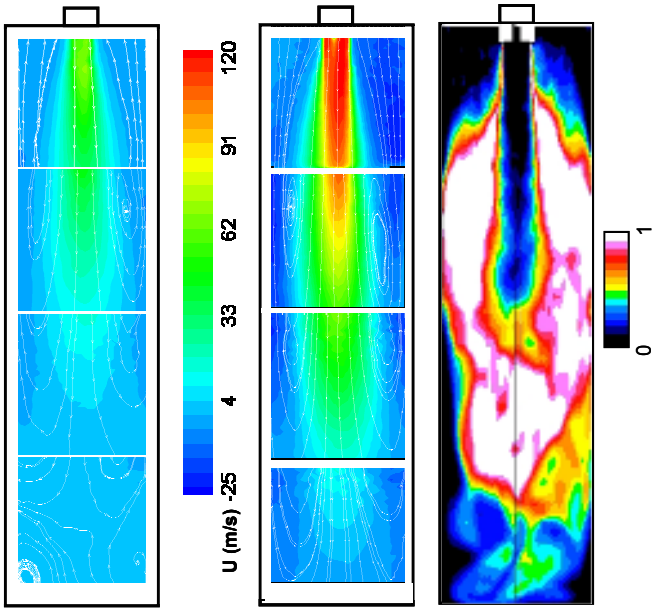

Figure 2. Mean axial velocity contour for (a) nonreacting flow (b)reacting flow. (c) Mean heat release contour– computational data.

In contrast for the reacting flow case (Figure 2b), the exiting product gases heat the incoming reactants to a temperature of approximately 500 K, which lowers the density and raises the velocities. Based on the measured preheat temperature, the expected velocity at the injector exit should be 129 m/s. Though the PIV data does not extend all the way to the injector exit plane, the measured average velocity at x=31 mm, where x is the axial distance from the injector exit, is only slightly slower at 122 m/s. The rapid decay in velocity results from the high shear between the incoming forward flow and the reverse flow of the exiting gases. On average, the incoming "jet" spreads rapidly, as evidenced by the diverging streamlines near the open end of the combustor. Due to the reduced density of the product gases, the return flow velocities are observed to be almost double that of the values obtained in the nonreacting flow. Essentially, the reverse flow increases the width of the shear layer compared to that a simple confined jet. Figure 2c shows the average (normalized) heat release predicted by the computations. The experimental results (not shown here) indicate that most of the heat release occurs in the center part of the combustor and does not become significant until 180-200 mm.[27] However, the computational result shows that most of the heat release occurs in the first half of the combustor in the shear layers close to the walls. This earlier heat release is likely due to the simple eddy-break up model and the adiabatic wall boundary conditions used in the computations.

Figure 3 shows the variation of mean axial velocity along the combustor centerline. In order to compare LES results with PIV, the simulations are first run for one flow through time to eliminate the transient effects and then averaged for another two flow through times. Overall, there is good agreement between the time-averaged LES and PIV data except in the region close to the exit of the injector. Although the location of the highest velocities agrees

well in the nonreacting flow case, the computations under predict the peak value in both reacting and nonreacting cases. This discrepancy is attributed to errors in the model predictions of the central recirculation zone just downstream of the closed fuel tube caused by modeling the tube as a short cavity, as well as differences in grid resolution between PIV and LES (the PIV resolution here is ~2 mm while the LES resolution is 100-200 microns).

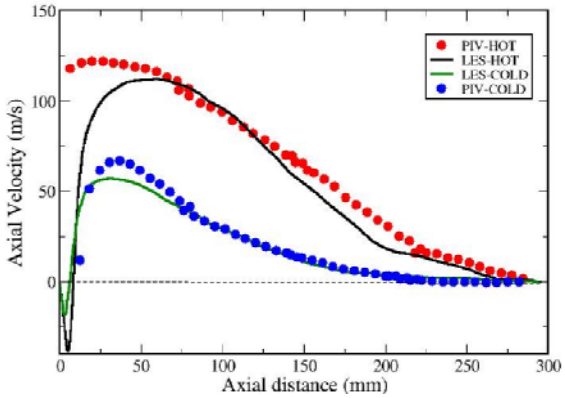

Figure 3. Variation of mean centerline axial velocity in nonreacting and reacting flow.

As the annular jet leaves the injector, it is slowed down by the presence of the cavity. This creates a small recirculation bubble at the tip of the injector. As the fluid moves downstream, the shear layers merge and the flow accelerates to its peak value. The axial velocity begins to decay rapidly as the flow approaches the stagnation end of the combustor. For the nonreacting flow, the centerline velocity drops to 2% of the peak value in approximately 2/3rd of the length of the combustor. The decay rate of the axial velocity is found to be higher than that of a free turbulent jet because of the effects of confinement as well as the presence of the stagnation plate at the end of the combustor. The centerline velocities for the reacting flow are approximately double the values obtained in the nonreacting flow. In the reacting flow case, the flowfield is changed significantly as a result of the effect of heat release and gas expansion on the fluid flow. Preheating of the incoming reactants by the hot product gases causes the higher flow velocities close to the injector while the presence of a flame zone and the consequent expansion results in higher velocities further downstream causing the flow stagnation to occur only at the base of the combustor. In the case of nonreacting flow, the PIV data indicates that on average, the stagnation region is located approximately one combustor diameter (70mm) upstream of the base plate. The heat release zone is also responsible for the slope change observed approximately 225mm downstream of the injector exit in the reacting flowfield. As noted previously, the location of primary heat release is underpredicted by the computations by approximately 40 mm compared to the experimental observations. Thus the slope change in the computational data also occurs ~40 mm before the PIV results. Although there is some discrepancy here, the average flow along the

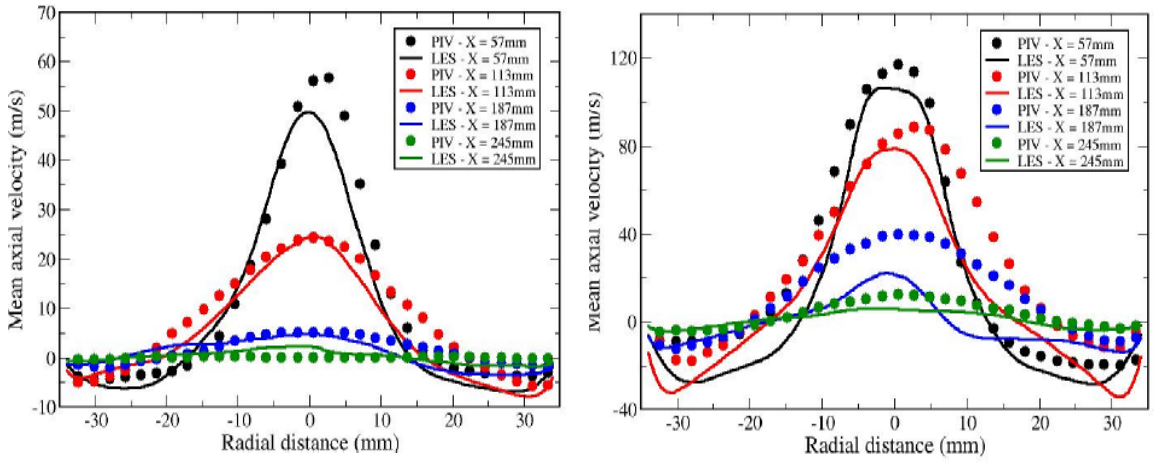

Figure 4. Comparison of radial profiles of u-velocity for (a) nonreacting and (b) reacting flow.

centerline is captured by the LES computations.

Figures 4a and 4b show comparisons of the radial profiles of mean axial velocity at four different axial locations between experiments and computations for the nonreacting and reacting cases. In both cases, the agreement between the PIV data and LES is satisfactory near the injector ($x < 150$mm), although the PIV data is slightly asymmetric. This is attributed to small imperfections in the injector or slight misalignment of the inner tube within the annular injector. For the nonreacting flow, the data is in good agreement with the computations through the entire length of the combustor. In the reacting flow, however, there is significant disparity between PIV data and LES results for the

x=187mm profile. This again can be attributed to the mismatch in the location of heat release. Beyond this point, the flow is affected by the presence of the stagnation region and slows down rapidly resulting in a more uniform profile near the lower end of the combustor. The reacting flow is characterized by significantly higher inlet/jet and return flow velocities as seen in Figure 4b. It is also observed that the return flow velocities predicted by the computations are higher in magnitude than the experimental data. This is because the computations use an adiabatic wall as the

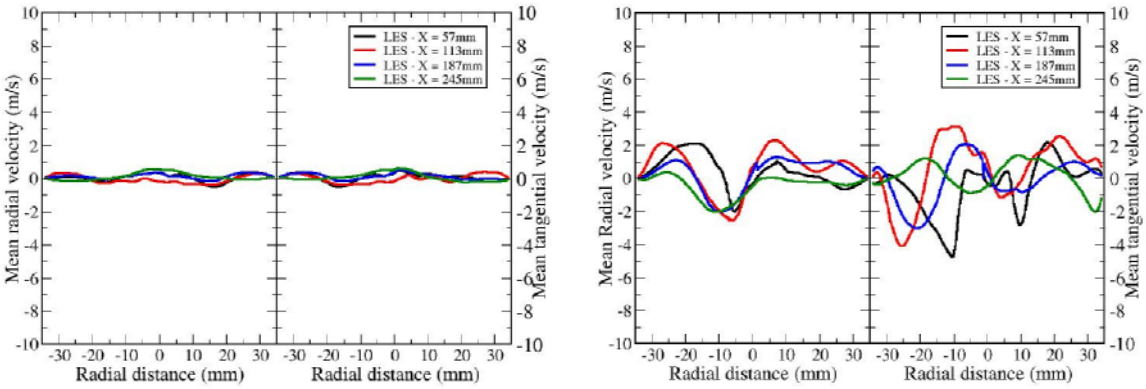

(a) **(b)**

Figure 5. Mean radial and tangential velocities for (a) nonreacting and (b) reacting flows.

boundary condition. Hence the higher temperature results in lower density product gases exiting the combustor at higher velocities. An interesting feature is that the radial velocity profiles becomes uniform around the same location (x = 245mm) in both the reacting and nonreacting flows though the absolute values are substantially higher for the reacting flow case.

Since a 2-d PIV set-up was used in this study and the timing was optimized to capture the high axial velocities, the uncertainty in v-velocity measurement is relatively high. Hence the computational data must be relied upon. Mean radial and tangential velocities for the nonreacting and reacting flow along a single diametrical cut are shown in Figures 5a and 5b respectively. It is clearly seen from the plots that the magnitude of the mean radial and tangential components are very small compared to the axial velocity magnitudes. Figure 5b shows that these

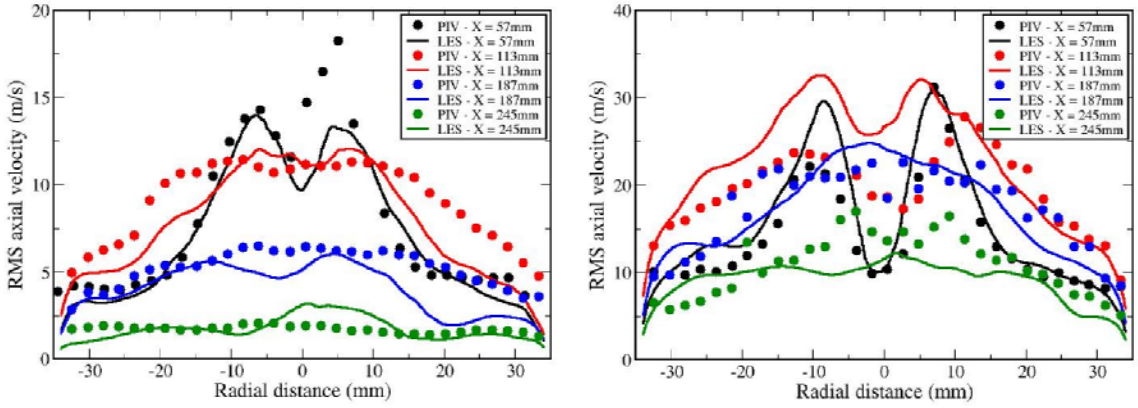

(a) **(b)**

Figure 6. Root mean square fluctuation of axial velocity for (a) nonreacting and (b) reacting flow.

velocities are higher in the reacting flow case. It is seen that the radial velocities follow the classic S-shape antisymmetric curve[7], providing a measure of validation of the computational predictions. However, there still appears to be significant noise in the results. For example, the average tangential velocities are expected to be zero for this nonswirling flow. Since the magnitude of the predicted average velocities are small compared to the average and instantaneous axial velocities, it is likely that the computations have not been run long enough for these values to attain convergence to zero.

The comparisons of axial RMS velocity profiles at different locations in nonreacting and reacting flow are shown in Figures 6a and 6b respectively. In the nonreacting flow case, the agreement between PIV and LES is

reasonably good near the injector and it improves further downstream. The peak RMS values are obtained in the shear layers where most of the turbulence is generated. The presence of the return flow results in high turbulence levels in the near field region of the injector and causes entrainment of product gases in this region. It is observed that the RMS velocity initially increases from x = 57 mm to x = 113 mm due to heat release after which there is a steady decay in the magnitudes towards the stagnation region. As the fluid moves downstream from the injector, the peaks in the rms velocity are smoothed out; but at the same time, the turbulence intensities steadily increase as the magnitude of the mean and rms velocities become comparable. Near the stagnation zone, the turbulence intensities are very high (~100%) implying that turbulent mixing is important in this region.

Figure 6b shows the corresponding values for the reacting flow case. Higher rms velocities are observed both in the forward and return flow regions of the reacting case. The rms velocities in the first two axial locations (57 and

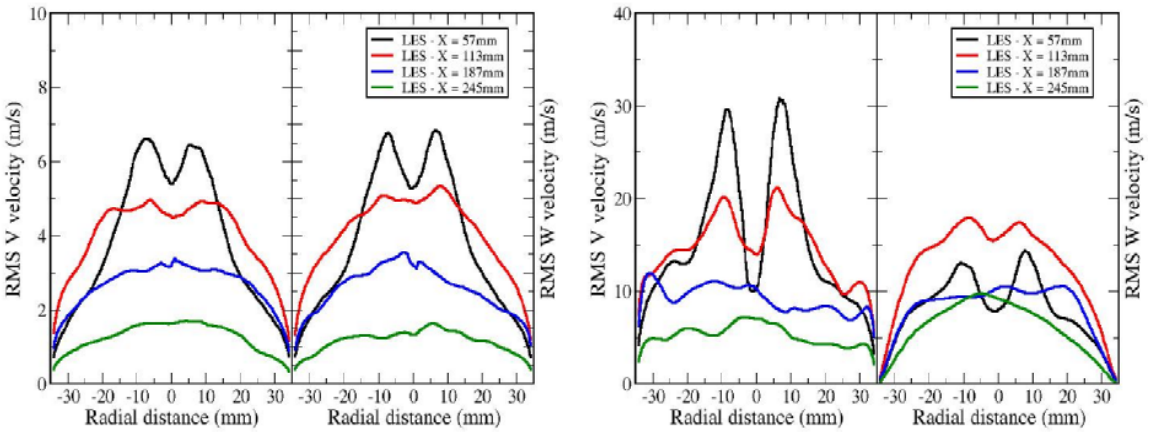

Figure 7. Radial profiles of root mean square fluctuations of v-velocity and w-velocity for (a) nonreacting and (b) reacting flow.

113 mm) are about double those found in the nonreacting case. Since the density decrease in the reacting case results in roughly doubling of the inflow jet velocity, this corresponds to nearly the same turbulence intensity as the nonreacting case. The increased shear in the reacting flow results in a correspondingly greater shear layer thickness. Farther downstream, however, much higher rms velocities and turbulence intensities are observed for the reacting case, even in the region closest to the end plate. This could result in additional turbulent mixing in the reacting case. Again the computations are in good agreement with the experiments for the nonreacting case, and also for the reacting case at the most upstream location. The computations overpredict the downstream velocity fluctations at x=113 mm, and underpredict them at the furthest downstream location. This again relates to the heat release discrepancy. The computational heat release begins and ends too far upstream, so the turbulence generation starts early and does not extend as far downstream.

Figures 7a and 7b show the variation of the (radial) v_{rms} and (tangential) w_{rms} velocities as predicted by the LES computations at different axial locations for the nonreacting and reacting flow. For the nonreacting flow, the v_{rms} and w_{rms} components are almost equal throughout the length of the combustor. Initially, the peak rms velocities are found in the jet shear layer. The u, v and w components of the rms velocity become comparable

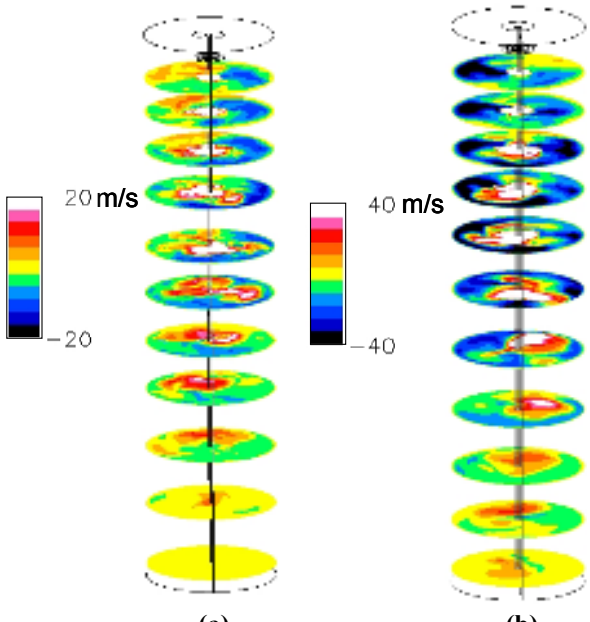

Figure 8. Instantaneous 3-D axial velocity contours for (a) nonreacting and (b) reacting flows.

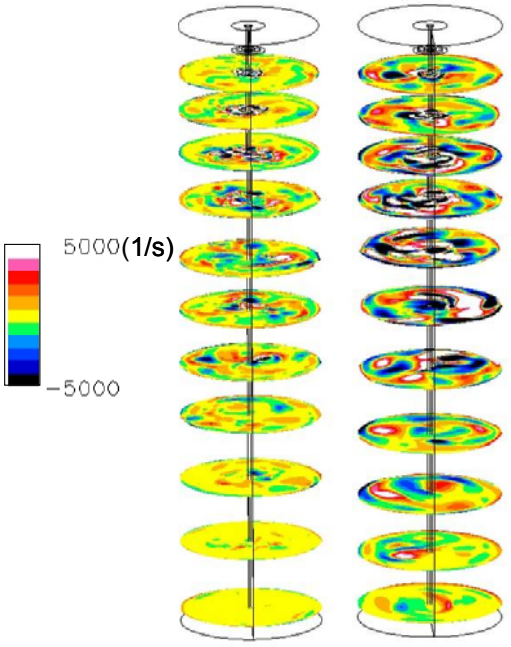

Figure 9. Instantaneous 3-D axial vorticity contours for (a) nonreacting and (b) reacting flows.

after roughly 2/3rd of the combustor length, i.e., where the mean axial velocity has nearly reached a stagnation condition. In this "stagnation" region, the rms velocities become comparable to the mean velocities and the turbulence intensities are quite high. As expected, the v_{rms} and w_{rms} velocities are higher in the reacting flow as compared to the nonreacting case (note the factor of four scale difference for the two cases). In the reacting flow case, radial (v) fluctuations are initially much higher than the tangential fluctuations. The v_{rms} and w_{rms} velocities become comparable in magnitude approximately 120 mm downstream of the injector, which is the region where heat release starts to be become significant in the computational results. In contrast to the nonreacting flow, the u, v and w fluctuations become comparable to each other much earlier, approximately at 1/3rd (x=100 mm) of the combustor length. The rms values, however, do not become comparable to the mean values until ~x=240mm. It should also be noted that the high rms values predicted by the computations appear to extend well into the return flow region and dissipate close to the walls, which may not be entirely physical.

To visualize the flow better, a 3-D view of the instantaneous axial velocity contours in the nonreacting and reacting flows are shown in Figures 8a and 8b. The instantaneous field shows the central core of the incoming gases maintaining a centered, jet-like structure in the nonreacting case. As the jet exits the injector, the core expands, slows down as we move further downstream and finally almost disappears after approximately 2/3rd of the combustor length. Below this region the axial velocities become negligible and the forward and reverse flow velocities are of comparable magnitude. There is some lateral movement of the jet, away from the centerline in the nonreacting flow, however this is not significant when compared to the reacting flow. Figure 8b shows the instantaneous axial velocity contours for the reacting flow. The velocity scaling is again doubled, since the incoming velocity is nearly doubled for the reacting case. Now the flow no longer maintains a simple centered jet-like form. The addition of heat release causes the jet to start breaking up at approximately 100 mm (1/3rd of the combustor length). Further downstream, around x=160mm (the region where the majority of heat release occurs), the central core of the jet has shifted laterally, almost to the edge of the combustor. The region of high forward (downward) velocity moves around the combustor, indicating that the jet is highly contorted. Smaller regions of medium forward velocity are observed almost all the way to the base of the combustor, where the flow must finally stagnate. The return flow velocities increase as the flow moves upwards from the stagnation region towards the exit, where there is clearly a region of high shear between the incoming and exiting flows. This is expected to produce strong entrainment of the product gases into the reactant stream. From a combustion point of view, it is known that this kind of exhaust gas recirculation helps enhance the formation of a radical pool and can hence improve the stability of the flame thereby enabling leaner operation of combustors.

Figures 9a and 9b show the instantaneous axial vorticity contours for the two cases at the same time instants as Figure 8. For the nonreacting case, there exists a pair of counter-rotating vortices in the shear layers on either side of the incoming jet. As the shear layers merge downstream, the vorticity is gradually dissipated and finally reduces to almost zero

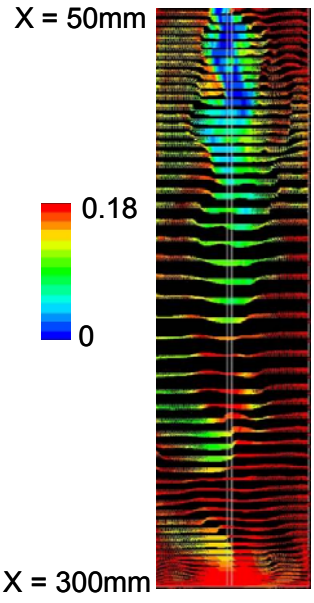

Figure 10. Instantaneous velocity vectors colored by contours of total product mass fraction.

midway through the combustor. For the reacting flow (Figure 9b), however, there is an increase in axial vorticity approximately 100 mm downstream of the injector. This rise in vorticity is believed to be due to the generation of baroclinic torque produced by the heat release/expansion in this part of the combustor. It is seen that axial vorticity persists almost all the way to the stagnation end of the combustor, although the magnitude is reduced away from the heat release zone.

All the above data shows the comparative effects of combustion on the flow field. Figure 10 shows instantaneous velocity vectors colored by the total mass fraction of products (CO_2, H_2O and CO). This provides a measure of product entrainment into the incoming jet of reactants. Most of the entrainment in this image occurs between x=50-100 mm, where the shear between the reactant and product streams is high. It is also observed that the incoming reactant jet either breaks up or gets highly distorted once the central core of the jet leaves the central axis of the combustor. Reactant packets appear to burn as pockets in regions surrounded by high concentration of products. It should be noted that large quantities of CO are formed near the shear layer, where the methane partial oxidation reaction takes place. The CO that is formed is then partly transported to the stagnation region while most of it is entrained back into the fresh reactant mixture in the recirculation zone.

Figure 11a shows an instantaneous temperature contour. The regions of the combustor near the injector exit exhibit a flame structure similar to a typical jet flame. However, as we move towards the central portion of the combustor, the flame structure is quite different. The corresponding instantaneous reaction rates are shown in Figure 11b. The high entrainment rates mix products into the incoming reacting flow thus resulting in a more uniform reaction zone. Thus the suppression of temperature spikes aids in lowering the NOx emission levels in this combustor.

Nonpremixed Reacting Flow

A distinguishing feature of the SPRF combustor is its ability to produce low emission levels even in the nonpremixed mode of operation. In this mode, the fuel is injected through the inner tube while the air enters through the annulus. Thus the fuel and air remain completely separated until they enter the combustor. This coaxial configuration enables the fuel to remain shielded from the return flow giving a chance for the fuel and air to mix with each other and with some products before burning. In the current study, the total mass flow rate and the overall equivalence ratio of the fuel and air are maintained at the same values as those used in the premixed experiments. It should be noted that computational work on the nonpremixed reacting flow is still in progress and that all the data shown in this section are experimental.

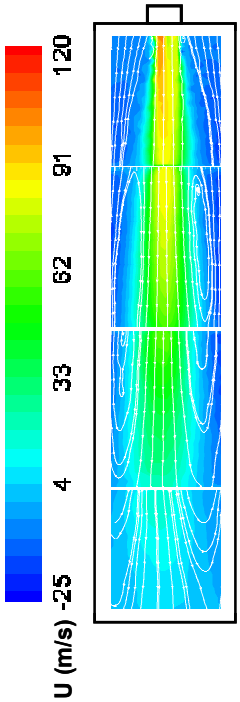

Figure 12. Mean axial velocity contours in nonpremixed reacting flow.

The average axial velocity contours (Figure 12), based on 400 individual realizations, indicate peak air velocities of the order of 90 m/s. It should be noted that the streamlines may appear discontinuous in some locations. This is because the streamlines are interpolated for each quarter of the combustor (since the data is acquired separately) and then assembled together. As in the premixed case, the velocity at the exit of injector is higher than the value calculated based on a cold (300 K) inlet mass flow rate. Preheating of the incoming air by the exhaust products flowing over the outside of the injector causes this increase in inlet velocity. Since the inner fuel tube is shielded by the air, the fuel has little preheating. The reverse flow velocities of the product gases are around 20 m/s. On average, there is also noticeable recirculation between the forward (jet) and reverse flows for x>75 mm, where x denotes axial distance from the injector exit.

The variations of the centerline mean axial velocities and the centerline axial rms velocities with axial distance for the nonpremixed reacting flow are compared against the values for premixed reacting flow in Figures 13a and 13b respectively. Nearer the open end of the combustor (x<100 mm), the centerline axial velocities are higher for premixed combustion. Initially, some difference would be expected due to the difference in inlet area (premixed operation utilizes only the annular passage of the concentric injector) and also due to small differences in the preheat temperature. In the nonpremixed reacting flow case, the inlet air temperature is measured to be 450 K (premixed inlet temperature was 500K) while the fuel is assumed to remain at approximately 300 K. Another reason for the velocity difference is

that flame is lifted in the nonpremixed mode of operation as opposed to the attached flame obtained in the premixed mode. Further downstream, the axial velocities are approximately equal, with the premixed mode exhibiting greater (centerline) velocity fluctuations. Except in the near field region of the injector, the jet decay rates are similar in the

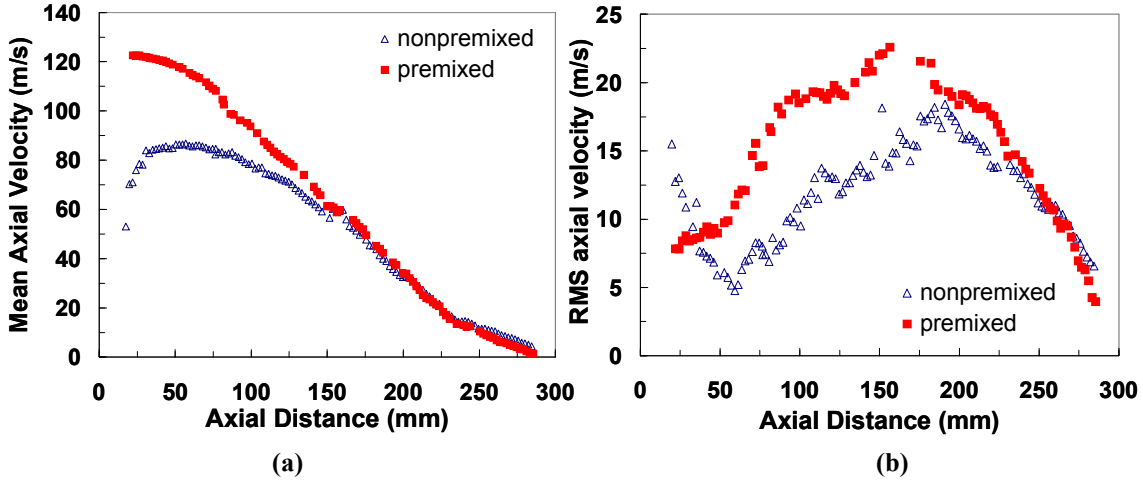

(a) (b)

Figure 13. Variation of mean axial velocity and axial RMS velocity along the centerline.

premixed and nonpremixed reacting flows. The variation of axial rms velocity along the centerline (Figure 13b) shows that the rms values are higher in the near field region of the injector exit for the nonpremixed case as compared to the premixed reacting flow case. This is caused by the interaction of fuel and air shear layers in the nonpremixed case. The high rms velocities enhance fuel-air mixing in this region. Downstream, the fuel-air shear layers merge in the nonpremixed case, reducing the rms velocities. Further downstream, the heat release becomes significant, causing a rapid rise in the centerline rms velocities in both the premixed and nonpremixed cases. The

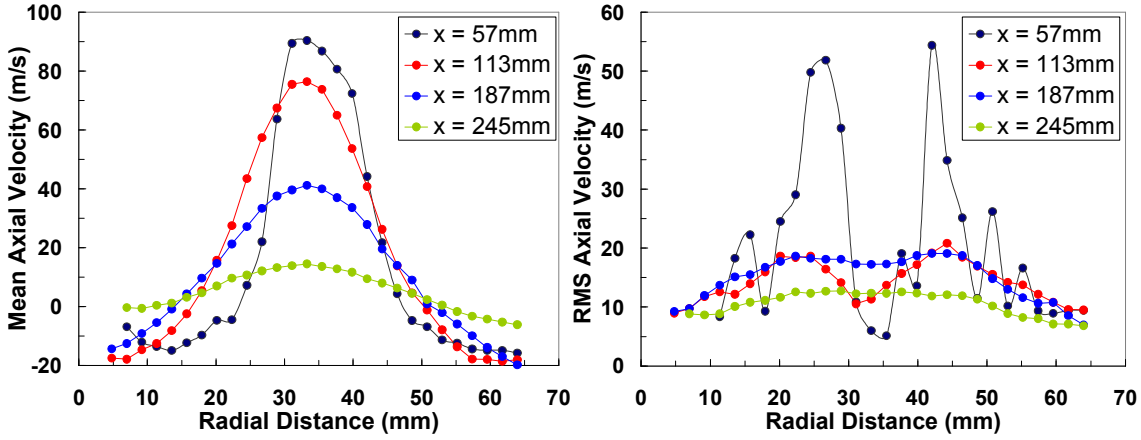

(a) (b)

Figure 14. Radial profiles of (a) mean axial velocity and (b) axial RMS velocity in nonpremixed reacting flow.

higher initial velocities in the premixed case result in higher rms values until approximately x=200 mm. Beyond this region, the mean and rms velocities of the premixed and nonpremixed flows are almost equal.

To compare the jet widths (defined based on the location where the velocity is equal to 50% of its peak value) and the shear layer thickness, the radial profiles of the mean axial velocity and the axial rms velocities for the nonpremixed reacting flow are shown in Figures 14a and 14b. The reader should note that data presented here is obtained experimentally and the lines connecting the data points are drawn only for the sake of clarity. Comparing Figure 14a with Figure 4b, it is seen that the initial jet widths are similar in both premixed and nonpremixed flows. Further downstream, the jet width is slighter higher in the nonpremixed case till approximately 2/3rd of the combustor length and this value remains almost constant beyond x = 187mm. At this point, the shear layers have

merged completely and further spreading of the jet is restricted due to the effects of confinement and by the presence of the return flow. The nonpremixed flow exhibits slightly higher return flow velocities due to the decreased area available to the return flow caused by the increased jet width compared to the premixed case. Figure 14b shows the radial profiles of the axial rms velocities. It is clearly seen that in the near field region, the nonpremixed flow has significantly higher rms velocities which is indicative of the presence of stronger shear layer compared to the premixed flow (Figure 6b). Therefore, the initial regions of the nonpremixed flow are highly turbulent and result in enhanced mixing rates. As we move away from the injector exit, the rms velocities become comparable to the premixed axial rms velocities. Hence it can be inferred that the overall flow features are similar in both premixed and non-premixed modes of operation except in the near field region of the jets. Therefore, the comparable performance of the combustor, in terms of emissions levels, in both premixed and nonpremixed modes of operation may be attributed to the similarities in flow fields and high levels of mixing.

V. Conclusions

The key features of the flowfield of a stagnation point, reverse flow (SPRF) combustor have been studied with the help of PIV and LES computations. The computations are in reasonable agreement with the PIV data in most cases. Although there are some small discrepancies, the authors believe that the model is able to capture the important physical features of the flow. The effects of confinement, flow reversal and combustion on the flowfield have been analyzed in detail. The presence of the closed combustor end and resulting return flow in the SPRF geometry affect the incoming jet flow significantly, as seen in the nonreacting results. The resulting "stagnation zone" near the closed end is a region of low mean velocity but significant fluctuating velocity. Near the closed end, the fluctuating and mean velocities become comparable, resulting in high turbulence intensities and enhanced mixing rates for both reacting and nonreacting flows. These properties are beneficial for flame stabilization.

Heat release and preheating of the incoming reactant jet by the exiting hot products are shown to significantly influence the flow field. They result in higher average and fluctuating velocities for both premixed and nonpremixed reacting cases as compared to the nonreacting flow. The nonreacting flow stagnates earlier than the reacting flow because of the gas expansion effects in the reacting flow case. Consequently the jet decay rates are higher for the reacting flow. The jet width and spreading rates in both the reacting and nonreacting flows are similar, which is due to the effect of confinement and the return flow. The computations of the instantaneous velocity and product mass fraction distribution clearly indicate entrainment and mixing of products into the reactant jet due to the high shear between the forward and reverse flows. Mixing of hot products into the reactants is another source of enhanced flame stability in the SPRF combustor.

Comparison of the instantaneous flowfields reveals that the reacting jet exhibits significant lateral motion and distortion compared to the nonreacting case. Thus the effect of heat release is to cause additional unsteadiness in the flow, which leads to increased mixing of products and reactants in the heat release regions. This is also evidenced by the instantaneous vorticity contours, which show increased vorticity and turbulence generation in the heat release zone. The temperature and reaction rate contours indicate the presence of broad reaction zones with uniform temperature distributions. The premixed and nonpremixed reacting velocity fields were found to be similar except in the near field region of the injector. Significant differences in the flowfield near the injector exit are due to the coaxial flow configuration in the nonpremixed flow. Mean and fluctuating centerline velocities in the near field region are lower for nonpremixed operation due to the differences in preheat and initial inlet areas. High fluctuating velocities in the near field shear layer of the nonpremixed flow result in enhanced mixing rates and high turbulence intensities causing the nonpremixed flow to behave similar to the premixed flow in the SPRF combustor.

Acknowledgments

This research is supported by NASA through the University Research, Engineering, and Technology Institute for Aeropropulsion and Power, under Grant/Cooperative Agreement Number NCC3-982.

References

[1]Gutmark, E., Parr, T. P., Hanson-Parr, D. M., and Schadow, K. C, "On the lean blow-out limit of premixed flames," AIAA-1989-154 Aerospace Sciences Meeting, 27th, Reno, NV, Jan. 9-12, 1989.

[2]Neumeier, Y., Weksler, Y., Zinn, B. T., Seitzman, J. M., Jagoda, J. and Kenny, J., "Ultra Low Emissions Combustor with Non-Premixed Reactants Injection," AIAA 2005-3775 41st AIAA/ASME/SAE/ASEE Joint Propulsion Conference & Exhibit 10 - 13 July 2005, Tucson, Arizona.

[3]C. J. Chen, and W. Rodi, Vertical *Turbulent Buoyant Jets; A Review of Experimental Data* - Pergamon, Oxford, 1980, HMT Vol. 4.

[4]List, E. J., Ann. Rev. Fluid Mech. 14, 189, 1982.
[5]Panchapakesan, N.R., and Lumley, J.L., "Turbulence measurements in axisymmetric jets of air and helium- Part 1. Air jet," J. Fluid Mech. 246 (1993) pp197-223.
[6]Hussein, H. J., Capp, S. P. and George, W. K., "Velocity measurements in a high-Reynolds-number, momentum-conserving, axisymmetric, turbulent jet," J. Fluid Mech. 258 (1994) pp31-75.
[7]Falcone, A. M., and Cataldo, J. C., "Entrainment velocity in an axisymmetric turbulent jet," Transactions of the ASME, Vol.125, July 2003 pp 620-627.
[8]Borean, J.L, Huilier, D., and Burnage, H., "On the effects of a co-flowing stream on the structure of an axisymmetric turbulent jet," Experimental Thermal and Fluid Science 17 (1998) pp 10-17.
[9]Chua, L. P. and Lua, A. C, " Measurements of a confined jet," Phys. Fluids, Vol. 10, No. 12, December 1998 pp 3137-3144.
[10]Panchapakesan, N. R., and Lumley, J. L.,''Turbulence measurements in axisymmetric jets of air and helium—Part 2. Helium jet,'' J. Fluid Mech. 246 (1993).
[11]Djeridane, T., Amielh, M., Anselmet, F. and Fulachier, L., "Velocity properties in the near-field region of axisymmetric variable density jets," Physics of Fluids (1996), 8, pp. 1615-1630.
[12]Serres, I., Chauveau, C., Sarh, B., and Gokalp, I., "Characterisation of confinement and impingement effects on the near field of axisymmetric jets using LDA and PIV," 10th International Symposium on Applications of Laser Techniques to Fluid Mechanics, Lisbon, Portugal 2000.
[13]Champagne, F.H. and Wygnansky, I.J. (1971). "An experimental investigation of coaxial turbulent jets," Int. J. Heat Mass Transfer, 14, pp.1445-1464.
[14]Dahm, W.A., Friedler, C.E. and Tryggvason, G. (1992). "Vortex structure and dynamics in the near field of a coaxial jet," Journal of Fluid Mechanics, 241, pp. 371-402.
[15]Durão, D. and Whitelaw, J.H. (1973). "Turbulent mixing in the developing region of coaxial jets," Transactions of the ASME-Journal of Fluids Engineering, pp. 467-473.
[16]Villermaux, E. and Rehab, H. (2000). "Mixing in coaxial jets", Journal of Fluid Mechanics, 425, pp. 161- 185.
[17]Yamaguchi, S., Ohiwa, N., and Kinoshita, S., "A study on opposed jet flames stabilized in a uniform air stream (1st report: Development of isothermal opposed jets.)," Bulletin of the JSME, Vol. 18, No. 121, July 1975.
[18]Yamaguchi, S., Ohiwa, N., and Kinoshita, S., "A study on opposed jet flames stabilized in a uniform air stream (2nd report: Mixing characteristics of an opposed jet.)," Bulletin of the JSME, Vol. 18, No. 121, July 1975.
[19]Sankaran, V., Gopalakrishnan, P., Undapalli, S., Parisi, V., Seitzman, J., and Menon, S., "A LES – PIV Investigation of a Stagnation Point Reverse Flow Combustor," AIAA2005-3969 41st AIAA/ASME/SAE/ASEE Joint Propulsion Conference & Exhibit 10 - 13 July 2005, Tucson, Arizona.
[20]Muniz, L., Martınez, R. E. and Mungal, M. G., "Application of PIV to turbulent reacting flows," *Developments in Laser Techniques and Fluid Mechanics* (Berlin: Springer) 2000 pp 411–424.
[21]Schumann, U., "Subgrid scale model for finite difference simulation of turbulent flows in plane channels and annuli," *Journal of Computational Physics*, Vol. 18, 1975, pp. 376-404.
[22]Menon, S., Yeung, P. K., and Kim, W. W., "Effect of subgrid models on the computed interscale energy transfer in isotropic turbulence," *Computers and Fluids*, Vol. 25, No. 2, 1996, pp. 165-180.
[23]Poinsot, T., Lele, S., "Boundary conditions for direct simulations of compressible viscous flow," *Journal of Computational Physics*, Vol. 101, 1992, pp. 104-129.
[24]Fureby, C., Lofstrom, C., "Large eddy simulations of bluff body stabilized flames," *Proceedings of the Combustion Institute*, Vol. 25, 1994, pp. 1257-1264.
[25]Orsino, S., Weber, R., "Numerical simulation of natural gas with high-temperature air," *Combustion Science and Technology*, Vol. 170, 2001, pp. 1-34.
[26]Westbrook, C. K., Fredderick L. D., "Simplified reaction mechanisms for the oxidation of hydrocarbon fuels in flames," *Combustion Science and Technology*, Vol. 27, 1981, pp. 31-43.
[27]Bobba, M. K., Gopalakrishnan, P., Radhakrishnan, A., Seitzman, J., Neumeier, Y., Zinn, B. T., and Jagoda, J.,"Flame stabilization and mixing studies in a novel ultra-low emissions combustor", AIAA-2006-963 44th AIAA Aerospace Sciences Meeting and Exhibit, Reno, Nevada. Jan 9-12 2006.